Available online www.jsaer.com

***Journal of Scientific and Engineering Research*, 2023, 10(5):141-158**

Research Article

ISSN: 2394-2630
CODEN(USA): JSERBR

Determination of Tectonic Lines of Hatay (Turkey) Region using Wavelet Method

A. Muhittin Albora

Istanbul University-Cerrahpaşa, Engineering Faculty, Geophysical Department, Büyükçekmece-Istanbul, Turkey Email: muhittin@iuc.edu.tr

Abstract the residual anomalies are the results of various depth and other properties of buried structures on gravity anomaly map. The superposition of anomaly of the underground structures with different properties such as depth, density and size increases the complexity of the overall system. Thus the extraction of the desired properties from the anomaly map becomes difficult. Different separation techniques are used to solve this problem. The wavelet transform is one of these modern approaches. Here, we tested various types of the wavelet transform and horizontal gradient modelling on synthetic example and then applied them to the gravity anomaly map of Hatay Region in Turkey. We have detected the borders of the Hatay Region and proposed tectonic model of this real complex structure using the wavelet transform and horizontal gradient together to support our results. We have found some important differences in our new model due to the previous studies on this region. The underground model of Hatay is also derived by two cross-sections.

Keywords Gravity anomaly map, Wavelet, Hatay region-Türkey, Tectonic

Introduction

At the last decades, the wavelet transform has many applications on geophysics. There are many researches on separation of potential anomalies and border detection of buried structures using wavelet approaches. The wavelets, first mentioned by Haar 1909, had compact support which means vanish outside of a finite interval. Haar wavelets are not continuously differentiable. In the 1930s, representation of function using scale-varying basis function that can vary in scale and conserve energy is researched by several researchers. Defined wavelet in the context of physics [1]. He gave a lift to digital processing by discovering pyramidal algorithms, and orthonormal wavelet basis [2]. He used Mallat's work to construct a set of wavelet orthonormal basis functions that are the cornerstone of wavelet application today [3]. They has first used the wavelet transform for potential-field data [4]. They have worked upon seismological data [5]. They had separated regional and residual potential-field anomalies using the wavelet transform [6]. They has separated potential anomaly data by wavelet approach [7]. They processed aeromagnetic data by the wavelet transform [8]. They have modelled geometric of geological bodies using multiscale edge analysis and forward modelling based on wavelet [9]. They have studied on de-noising of signals from potential field effects and tried to estimate borders of the buried objects [10]. They have also detected the borders of underground geological bodies using wavelet transform [11]. They have applied wavelet approach to archaeological sites and estimated the borders of ancient cities [12, 13].

The studying area the African, Arabian and Anatolian block (part of the Eurasian Plate) interacting in North Eastern Mediterranean which is one of the most complex tectonic zones along the Alpine-Himalayan orogenic belt (Figure 1). East Anatolian and Dead Sea Faults (DSF), Bitlis Suture and Cyprus Arc are the main neotectonic structures of North-Eastern Mediterranean area. The East Anatolian Fault Zone is a 550 km-long, approximately northeast trending, left-lateral strike slip-character fault zone [14]. The total observed displacement along this fault is about 3.5-13 km on displaced Euphrates River channels and 15-27 km on displaced pre-Pliocene units [15, 16]. They proposed 35-40 km offset on the East Anatolian Fault Zone [17]. The left-lateral fault system in the region N-S trending and 1000 km-long is Dead Sea Fault Zone (DSFZ) which extends from the Red Sea to the Tauride Mountains and forms the western edge of the Arabian plate [18]. DSFZ is active since Middle Miocene time and the total offset values changing between 105-107 km and 10-20 km are obtained from different segments [19]. In this paper, a very complex geological structure in Hatay Region is investigated using wavelet approach. Although some of the faults can be observed on the gravity anomaly maps, particularly DSF with strike-slip component cannot be evaluated without powerful image processing techniques. They have tried to detect faults in the region using stratigraphic, tectonic and seismic data [20]. They have studied on volcanic activities of Hatay region and investigated tectonism of Anatolian and Arabic plates [21]. They have found geological map of this region using drillings [22]. They have extracted effective tensions by research on earthquakes [23]. They have studied on Amanos fault kinematics [24]. The left-lateral Amanos Fault follows an escarpment that bounds the eastern margin of the Amanos mountain range and the western margin of the Karasu Valley in southern Turkey. They have identified the left-lateral displacement on the Nort-Anatolian Fault Zone (NAFZ) from seismological, geological and kinematic studies [25, 26, 27, 28]. They have studied fault kiematic analysis and inversion of focal mechanisms of shallow earthquakes of the regional stress regime in the northeastern most corner of the Eastern Mediterranean region [29]. Here, we have also analysed the tectonic structure and proposed a new fault model of this considered area using wavelet transform approach for modelling various faults of Hatay Region.

Method

Wavelet Transform and Gradient Aprroaches on Synthetic Examples

In this Section, the performance of the wavelet transform and gradient approaches will be analysed on synthetic examples. Especially the capacity of the wavelet transform will be tested for boundary extraction of various buried structures resulting gravity anomalies.

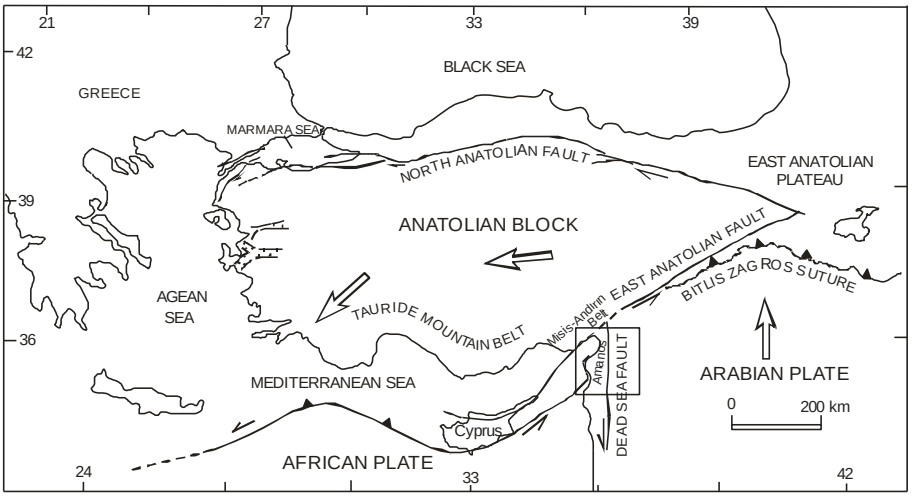

Figure 1: Simplified tectonic map of the Anatolian region and surroundings showing the main tectonic domains developed during Miocene to Holocene time. Lines with filled triangles show active subduction zones, the ones

with open triangles are active thrusts at continental collision zones, and lines with tick marks are normal faults. The large solid arrows indicate the sense of motion of the lithospheric plates.

Wavelet Transforms

The classes of functions that present the wavelet transform are those that are square integrable on the real line. This class is denoted as $L^2(R)$,

$$f(x) \in L^2(R) \Rightarrow \int_{-\infty}^{+\infty} |f(x)|^2 \, dx < \infty . \tag{1}$$

The set of functions that are generated in the wavelet transform are obtained by dilating (scaling) and translating (time shifting) a single prototype function, which is called the mother the wavelet transform. The wavelet transform function $\psi(x) \in L^2(R)$ has two characteristic parameters, called dilation (a) and translation (b), which vary continuously. A set of wavelet basis function $\psi_{a,b}(x)$ may be given as

$$\psi_{a,b}(x) = \frac{1}{\sqrt{|a|}} \psi\left(\frac{x-b}{a}\right) \qquad a, b \in R \, ; a \neq 0 . \tag{2}$$

Here, the translation parameter, "b", controls the position of the wavelet in time. The "narrow" wavelet can access high frequency information, while the more dilated wavelet can access low frequency information. This means that the parameter "a" varies for different frequencies. The continuous wavelet transform is defined by

$$W_{a,b}(f) = < f, \psi_{a,b} > = \int_{-\infty}^{+\infty} f(x) \psi_{a,b}(x) \, dx . \tag{3}$$

The wavelet coefficients are given as the inner product of the function being transformed with each basis function.

He invented one of the most elegant families of wavelets [3]. They are called compactly supported orthonormal wavelets, which are used in discrete wavelet transform (DWT). In this approach, the scaling function is used to compute the ψ. The scaling function $\phi(x)$ and the corresponding wavelet $\psi(x)$ are defined by

$$\phi(x) = \sum_{k=0}^{N-1} c_k \, \phi(2x-k) , \tag{4}$$

$$\psi(x) = \sum_{k=0}^{N-1} (-1)^k \, c_k \, \phi(2x+k-N+1) , \tag{5}$$

where, N is an even number of wavelet coefficients c_k, k= 0 to N-1. The discrete presentation of an orthonormal compactly supported wavelet basis of $L^2(R)$ is formed by dilation and translation of signal function $\psi(x)$, called the wavelet function. Assuming that the dilation parameters "a" and "b" take only discrete values. $a = a_0^{\,j}$, $b = k b_0 a_0^{\,j}$. Where $k, j \in Z$, $a_0 > 1$, and $b_0 > 0$. The wavelet function may be rewritten as

$$\psi_{j,k}(x) = a_0^{\,-j/2} \, \psi(a_0^{\,-j} x - k b_0) , \tag{6}$$

and, the discrete-parameter wavelet transform (DPWT) is defined as

$$DPWT(f) = < f, \psi_{j,k} > = \int_{-\infty}^{+\infty} f(x) a_0^{-j/2} \psi(a_0^{-j} x - k b_0) dx, \quad (7)$$

He introduced an efficient algorithm to perform the DPWT known as the Multi-resolution Analysis (MRA) [2]. It is well known in the signal processing area as the two-channel sub-band coder. The Multiresolution representation is linked to Finite Impulse Response (FIR) filters. The scaling function ϕ and the wavelet ψ are obtained using the filter theory and consequently also the coefficients are defined by these last two equations. If at $x=t/2$, $F\{\phi(x)\}$ is considered and

$$\Phi(\omega) = H\left(\frac{\omega}{2}\right)\Phi\left(\frac{\omega}{2}\right), \quad (8)$$

The idea is to first form a 1-D sequence from the 2-D image row sequences, do a 1-D MRA, restore the MRA outputs to a 2-D format and repeat another MRA to the 1-D column sequences. The two steps of restoring to a 2-D sequence and forming a 1-D column sequence can be combined efficiently by appropriately selecting the proper points directly from the 1-D MRA outputs. As seen in Figure 2, after the 1–D row MRA, each lowpass and highpass output goes through a 2-D restoration and 1-D column formation process and then move on to another MRA. Let t_1 and t_2, be the 2-D coordinates and L=lowpass, H=highpass. Then the 2-D separable scaling function is,

$$\phi^{(1)}(t_1, t_2) = \phi(t_1)\phi(t_2), \quad LL \quad (9)$$

original signal can be reconstructed. Then 2-D separable wavelets are,

$$\psi^{(2)}(t_1, t_2) = \phi(t_1)\psi(t_2), \quad LH \quad (10)$$

$$\psi^{(3)}(t_1, t_2) = \psi(t_1)\phi(t_2), \quad HL \quad (11)$$

$$\psi^{(4)}(t_1, t_2) = \phi(t_1)\phi(t_2), \quad HH \quad (12)$$

The scheme of separable 2-D processing, while simple and uses available 1-D filters, has disadvantages when compared to a genuine, 2-D MRA with non-separable filters. The latter possesses more freedom in design, can provide a better frequency and even linear phase response, and have non-rectangular sampling (Figure 2).

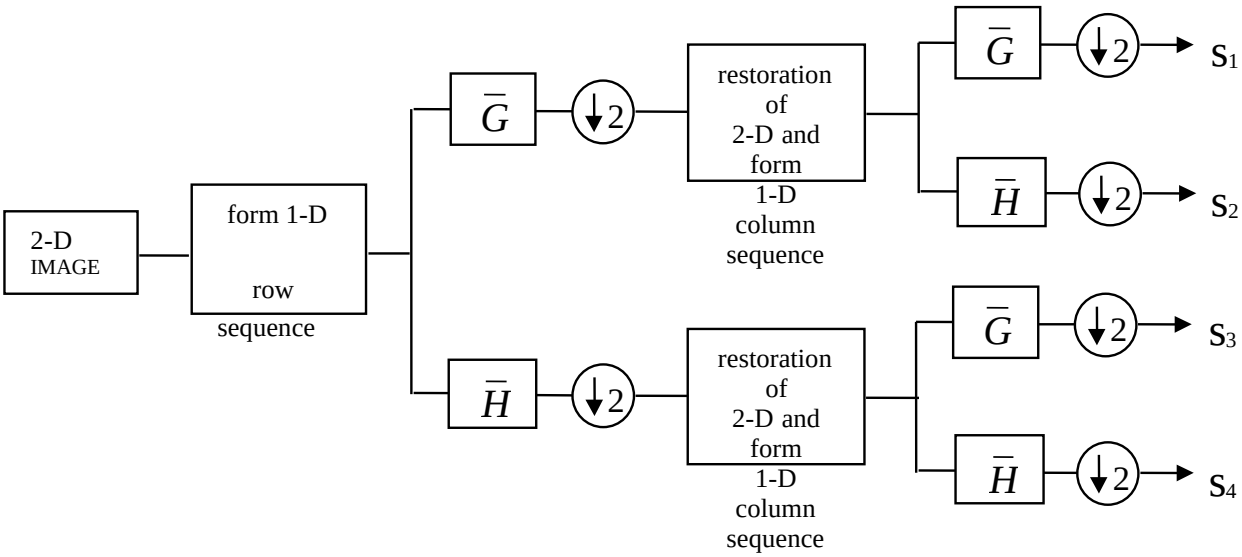

Figure 2: 2-D Multi-resolution analysis

Wavelet transform application on synthetic example

We have applied the wavelet transform approach to synthetic examples given by Figure 3 and 4. Our aim is to extract the borders of the synthetic prisms. At the output of the wavelet transform image processing tecnique, the borders are detected clearly. Here a synthetic model is given where two prisms are placed perpendicular with 0.5 gr/cm^3 density contrast, resulting the anomaly (Figure 3a0). We have shown wavelet outputs of these prisms in Figure 3a1 and wavelet tranform components are also given. At the horizontal wavelet tarnsform output, the differences at the horizontal borders are clearly shown (Figure 3h1). Thus the separation of two prisms in horizontal axes is achieved. In Figure 3v1, vertical wavelet transforms' outputs, which is calculated from prisms anomalies are given. In the peer observation of the vertical the wavelet transform output; it is clear that the anomalies are focused on the vertical sides. This is one of the advantages of the wavelet transform. At the diagonal the wavelet transform output, the corners of the prisms are observed (Fig. 3d1). On the output of wavelet transform, we palaced symbols obtained by boundary analysis to comfirm the result of of two approaches. The other wavelet transform outputs are shown in a2, a3 ve a4 for various levels. The horizontal, vertical and diagonal components are shown in Figure 3 as h2, h3, h4; v2, v3, v4 and d2, d3, d4 respectively. As level numbers are increased, distortion is also increases. Thus the optimum outputs are obtained for first and second levels.

The prisms in Figure 3a are rotated as 45 degrees and then gravity anomaly is obtained as in Figure 4a0. The aim of choosing this example with 45 degrees of rotation is to evaluate the performance of the wavelet transform in this special case. Wavelet outputs of horizontal placed prisms are given in Figure 4a1, a2, a3. Here, resolution decreases as the levels increase. At the output of horizontal the wavelet transforms (Figure 4h1, h2 and h3), the anomalies are observed on longitude axes. The symmetry property of the anomalies is vanishing as reaching vertical sides. In Figure 4v1, v2 and v3, vertical the wavelet transform output is shown. The results are similar to horizontal the wavelet transforms (Figure 4h1). In Figure 4d1, d2 and d3, diagonal the wavelet transform output is given. Here the corner points correspond to diagonal of Figure 3. Thus at diagonal the wavelet transform output in Figure 3d1 the corners of the structure are clearly detected. In Figure 4d1, diagonal the wavelet transform gives the longitude sides of the structures because of its being 45 degrees rotation.

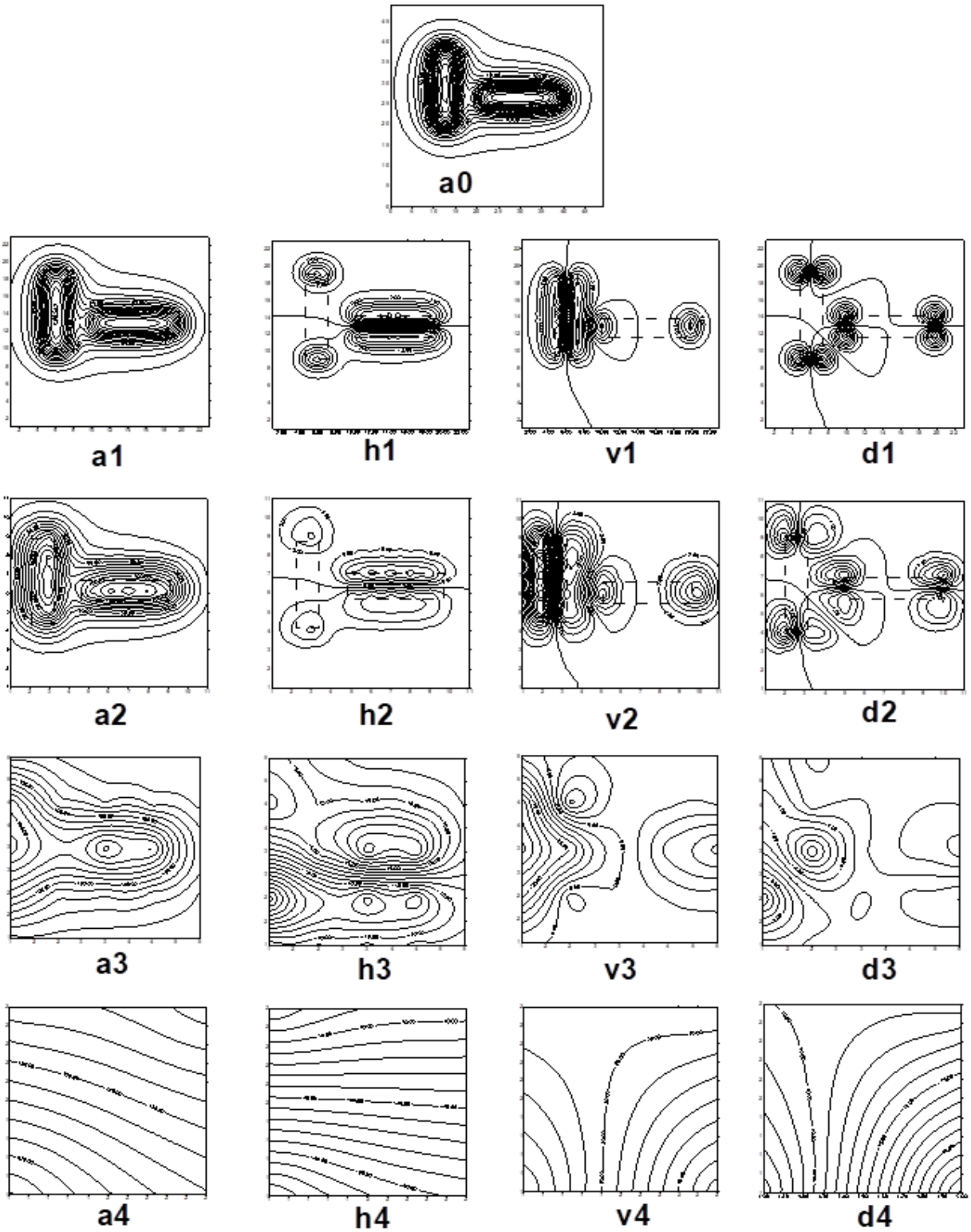

Figure 3: Synthetic example with two perpendicular prisms (a0). Bouguer anomaly (a1, a2, a3, a4). Wavelet outputs of Bouguer anomaly map (h1, h2, h3, h4). Horizontal component (v1, v2, v3, v4). Vertical component (d1, d2, d3, d4). Diagonal component.

Thus anomalies are obtained at along the longitude sides. The edges of the synthetic example are represented by maximum and minimum values of the horizontal and vertical the wavelet transform outputs (Figure 4h1 and v1). In diagonal the wavelet transforms output (Figure 4d1), zero contour surrounding maximum anomaly, and gives the information of structure edges. As a result, we can say that these two synthetic examples can represent most of the possible configurations of these kinds of structures in the field.

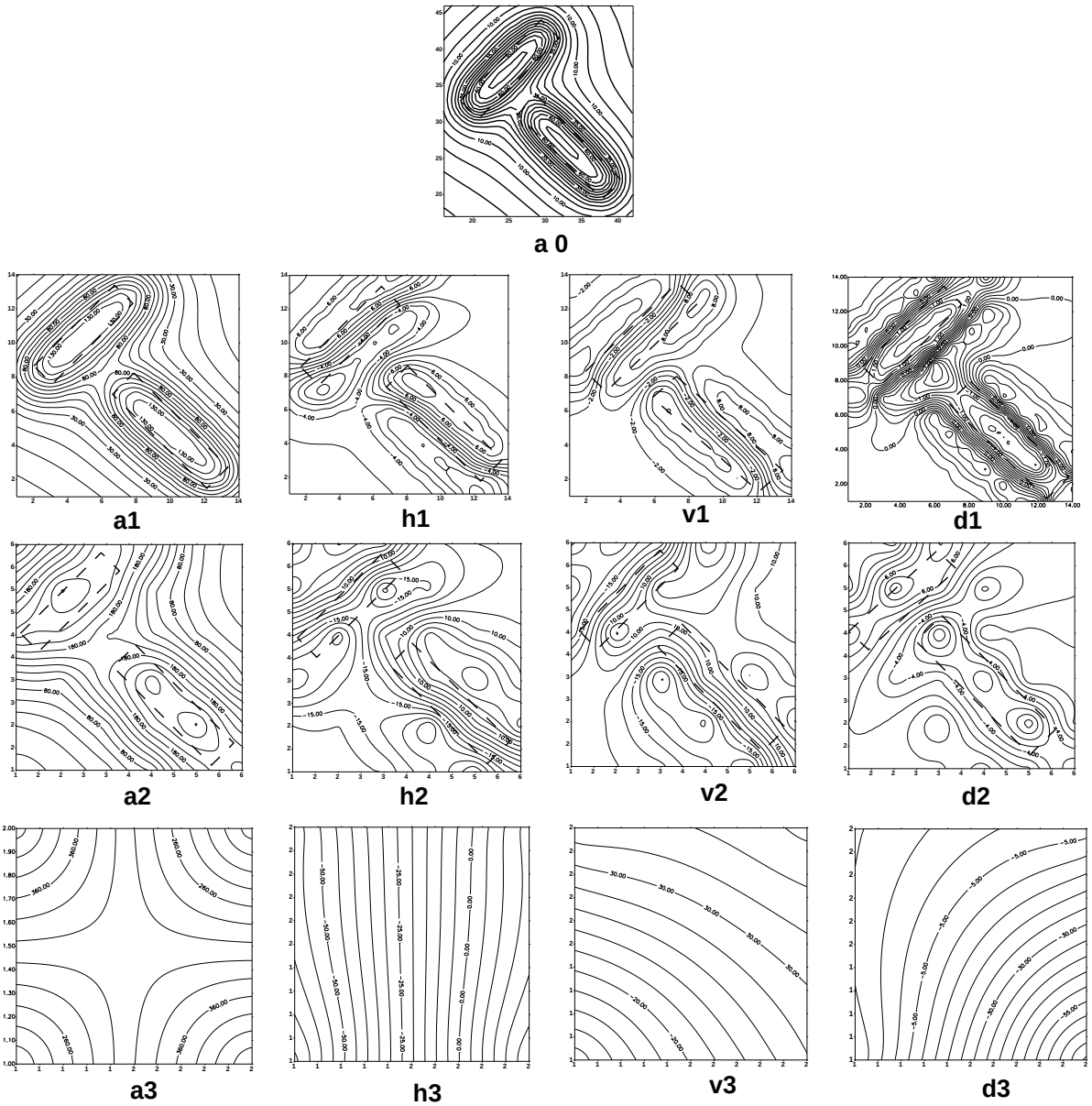

*Figure 4: Synthetic example with prisms with 45 degrees diversion. (**a**0). Bouguer anomaly (**a1, a2, a3).** Wavelet outputs of Bouguer anomaly map (**h1, h2, h3).** Horizontal component (**v1, v2, v3).** Vertical component (**d1, d2, d3).** Diagonal component.*

Horizontal gradients and Boundary analysis

The instant changes at the density of the buried objects result instant anomalies and these kind of instant deviations can be detected by the gradient-based algorithms. The horizontal gradient of the gravity anomaly is given as,

$$h(x,y)=\left[\left(\frac{\partial g_z(x,y)}{\partial x}\right)^2+\left(\frac{\partial g_z(x,y)}{\partial y}\right)^2\right]^{1/2} \quad (13)$$

They horizontal gradient can be solved by the simple finite difference approaches [30]. They have developed a software program in detecting the maximum values of a buried object using horizontal gradient based on algorithm expressed in Equation 13. Here we have used this classical approach for evaluation of both synthetic and real data.

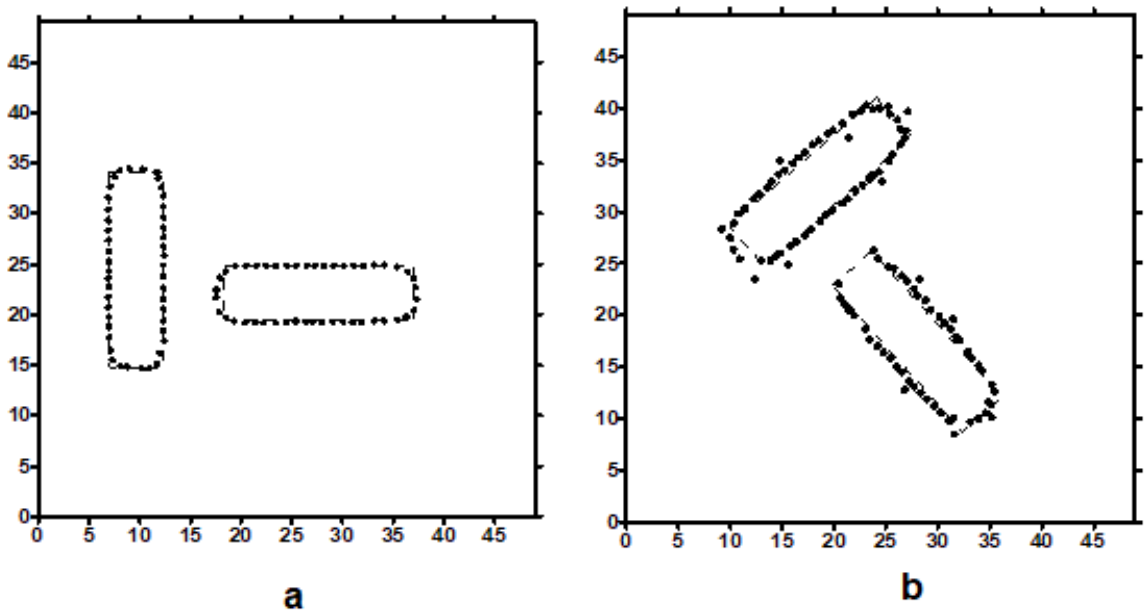

Figure 5: Gradient outputs of synthetic examples in Figure 3-4. (a). Horizontal gradient in figure 3a0 (b). Location of the maximum horizontal gardient in Figure 4a0.

Gradient Approach Application on Synthetic Examples

We have tested this classical approach by using similar synthetic examples given in Figure 3a and 4a. The gradient algorithm output is shown in Figure 5a and 5b. We replaced different coloured symbols due to the maximum anomaly values obtained from the horizontal gradient to clarify the borders (Figure 5a and 5b). In the observation of these Figures, the borders are clearly detected. We have also placed the maximum values of horizontal gradient on the wavelet transform outputs (Figure 3 and 4). We use the wavelet transform approaches and boundary analysis on the same Figures, but our aim is not to compare them. We try to model and enhance the detection of the borders of the structures with different approaches supporting similar results. Thus we are able to evaluate the wavelet transform and gradient based classical approaches for synthetic various examples.

Geology and Tectonic Structure of Hatay

In Hatay Region, young tectonic movements have formed Amanos Mount, Iskenderun Bay and Hatay graben. In the South of Amanos Mountains, a continuous ophiolite succession, the Kizildag ophiolite, is exposed from tectonite peridotites, through layered and isotropic gabbros to the sheeted dike complex and pillowed volcanics [31]. Here, the young tectonic movements are taken into consideration, starting from Arabia to North-North East and Anatolian block movements to West. Dead Sea Fault (DSF) zone is a tectonic structure with 1000 km in length starting from Dead Sea and ending at Hatay [32, 33, 34]. DSF, starting from Maras, tending to South-

North to Dead Sea, is the main fault system forming Hatay graben. It is assumed that DSF is formed as a rift of Arabian plate and Africa plate and their rotation to North with counter clockwise of 6-7 degrees [25, 35, 36, 37]. They estimated the slip rate on the Arava segment of the Dead Sea Fault Zone (DSFZ) as 4 ± 2 mm a^{-1} [38]. He predicted the slip rate, as slip rate on the southern DSF is 4 mm a^{-1} using DSF geology and GPS data [19]. This displacement has resulted left lateral faults from South to North. In Hatay, Amik area is Pliyo-Kuvaterner with 30 km length [37, 39]. The force forming the fault has also affected the sedimentary rocks, which lie on the West and East of the fault with 90 degrees angle [21]. DSF is more effective in Syria than in Turkey since it is covered by Amik plane composed of alluvial in Turkey [40]. West graben fault is the region of Kahramanmaras and Kirikhan and surrounded by East of Amonos Mountains and vertical shift is dominant (Figure 6). Erzin–Iskenderun fault, which makes Amanos Mountains to be seen as horst forms listric faults in Iskenderun basin [41]. The faults start from Hatay and reach to Samandagı [42] (Figure 6).

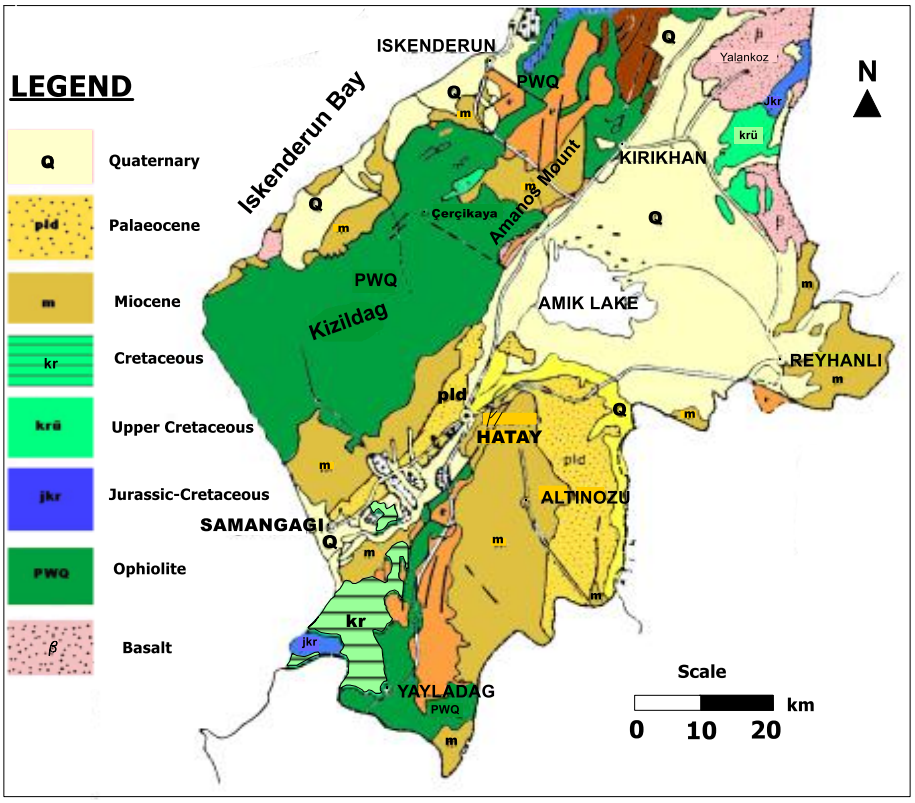

Figure 6: Geological map Hatay (The original map is obtained from Technical Ore Research of Turkey [43]).

Earthquake Activity

Türkiye is located on many active fault lines tectonically. Large earthquakes occur due to Turkey's complex tectonic regime. Because the focal mechanisms of the earthquakes are close to the surface, earthquakes are quite destructive. The relative movement of the Arabian, Eurasian and African plates creates complex fault systems in Anatolia. Continental collision causes N-S compression in eastern Turkey. It moves towards the west of Anatolia. Between Eurasia and Anatolia, the North Anatolian Fault Zone (NAFZ) extends ~1500 km from the Karlıova Triple Junction in the east to the Aegean Sea in the west. There have been many destructive earthquakes greater than 7 on the fault. On the other hand, the left lateral Dead Sea Fault Zone (DSFZ) and the East Anatolian Fault Zone (EAFZ) meet at the Maraş Triple Junction in eastern Turkey. The EAFZ stretches for 600 km from Hatay in the southwest to Karlıova in the northeast. According to historical records, the region has been formed by many destructive earthquakes. [44, 45], estimate geological and kinematic of North Anatolian

Fault Zone (NAFZ) and show dextral, sinistral slip senses along them. There are two earthquakes greater than 7 in Hatay Region. These are: 13 August 1822 and 3 April 1872 [34]. On February 6, 2023, a disaster occurred in Turkey. Two of the most destructive earthquakes of the century (Mw 7.8 and Mw 7.7) occurred at 04:17 and 13:24, Turkey time, with epicenters in Pazarcık (Kahramanmaraş) and Elbistan (Kahramanmaraş). BMw 7.8 struck the eastern part of the country at 04:17 local time. Unexpectedly, nine hours later, the second Mw 7.7 mainshock shook the area. These earthquakes destroyed numerous cities and villages in 11 provinces, including major major and economically important cities such as Kahramanmaraş, Hatay, Adıyaman, Malatya, Adana and Gaziantep. The latest official information in March 2023 shows that more than 270 thousand residential buildings and 60,000 commercial buildings were completely destroyed or severely damaged, with more than 60,000 deaths Figure7.

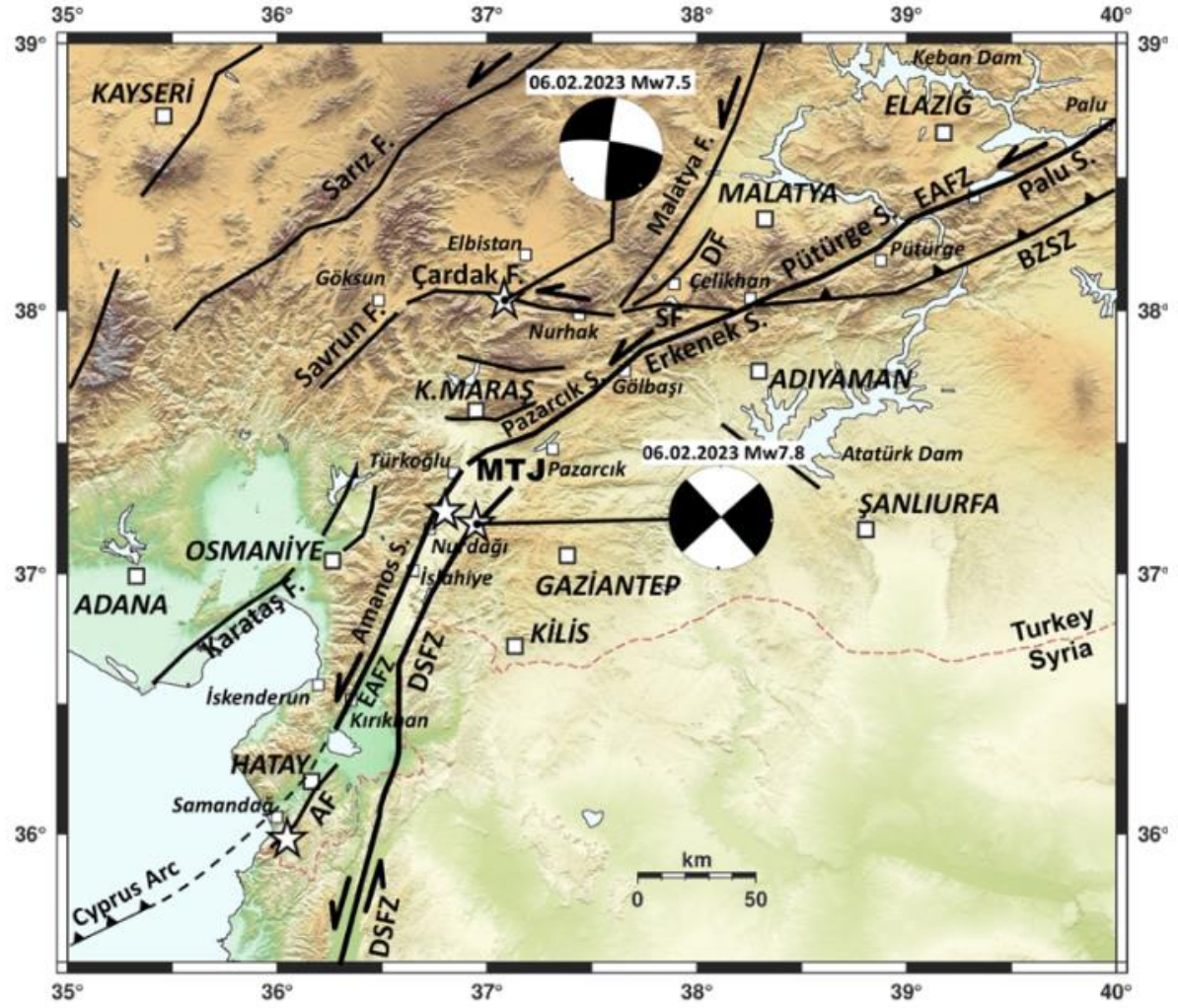

Figure 7: Main tectonic features based on the MTA fault map (Emre et al. 2013; Modified from Tan 2023). Focal mechanism solutions are from USGS. White arrows are plate motions. AF: Antakya Fault, BZSZ: Bitlis-Zagros Suture Zone, DF: Doğanşehir Fault, DSFZ: Dead Sea Fault Zone, EAFZ: East Anatolian Fault Zone, MTJ: Maraş Triple Junction, SF: Sürgü Fault [46].

Following these earthquakes, on 20.02.2023 at 20:04 local time, an earthquake with a magnitude of Mw 6.4 and a depth of 16 km, the epicenter of which was in Defne (Hatay), occurred. 20.02.2023 A series of earthquakes with magnitudes ranging from Mw 3.0 to 5.2 occurred in the 20-hour period after Mw 6.4 of the Defne (Hatay)

earthquake (Figure 8). According to the earthquake focal mechanism solutions published by various national and international seismology centers, it was evaluated that the earthquake in question was caused by a north-east-southwest-sloping normal fault with a left-lateral strike-slip component and dipping to the northwest. The focal mechanism solutions of the main earthquake, the sequences of the main and aftershocks indicate that the source fault of the 20.02.2023 Defne Hatay Mw 6.4 earthquake may be the northern part of the Antakya Fault Zone. The Antakya Fault Zone is an active oblique-slip fault zone extending from the northeast of Antakya to the west of Yayladağı, generally consisting of North and South fault segments, presenting a fragmented geometry in places, extending in the general direction of N40°E and dipping to the northwest. Along the fault zone, Cenozoic-Mesozoic aged basement rocks in the east and the current sediments of the Asi River forming the Antakya Plain came face to face. The current deposits in question consist of unconsolidated, water-saturated young sediments that are prone to liquefaction, represented by alluvium, where the Orontes River bed is located).

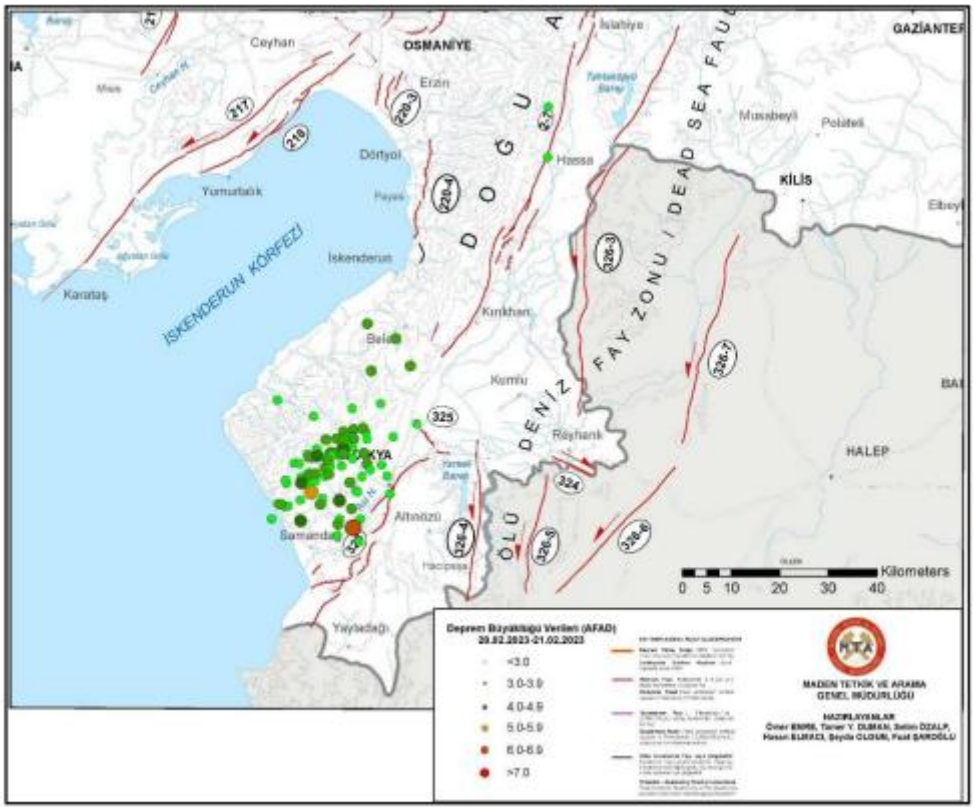

Figure 8: Distribution of the earthquake that occurred in Defne (Hatay) on February 20, 2023 and its aftershocks on the Turkey Active Fault Map (MTA, 2013). Seismological data were obtained from AFAD [47].
Application of Wavelet Transform and Horizontal Gradient Approaches to Bouguer Anomaly of Hatay Region

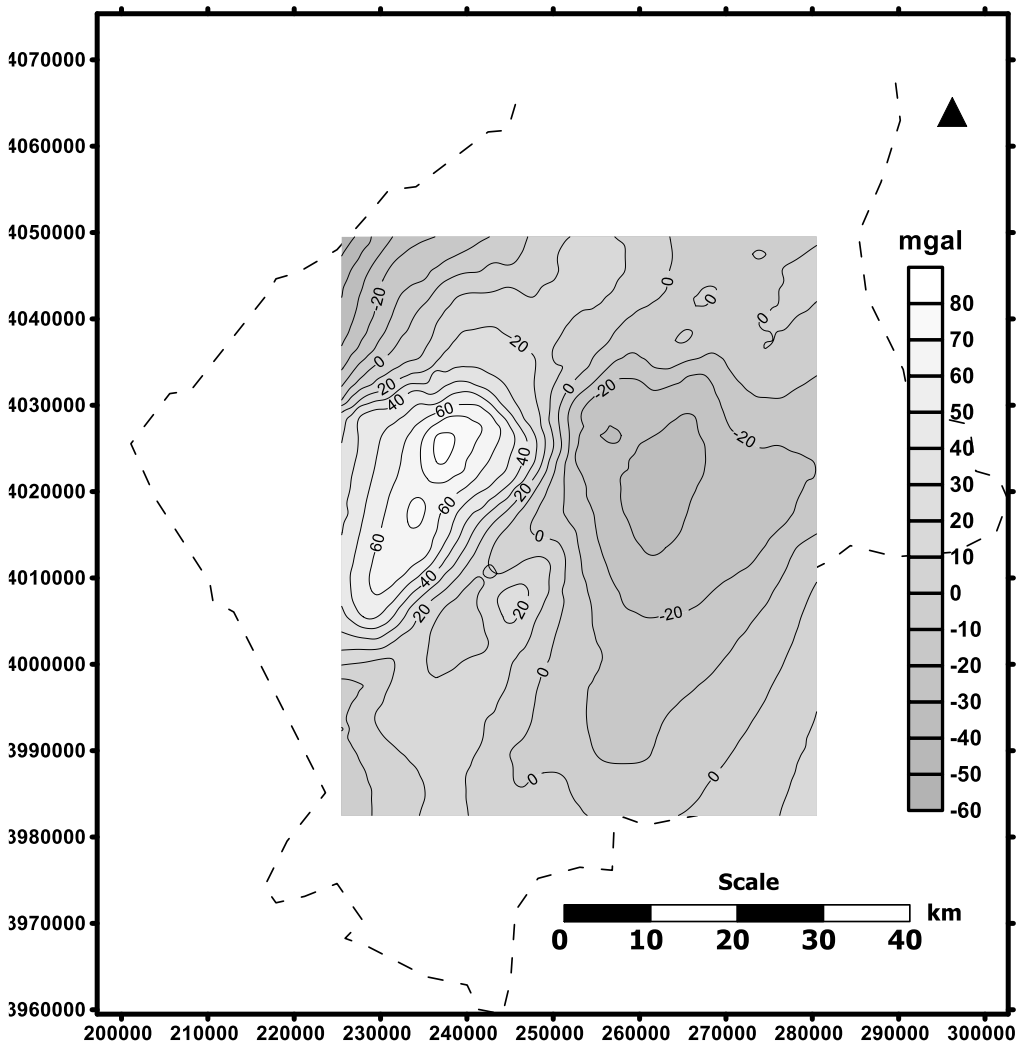

Figure 9: Bouguer anomaly map in Hatay region Contour interval is 10 mgal (The original map is obtained from Turkish Petroleum Cooperation, TPAO).

In Bouguer anomaly map of Hatay (Figure 9), -35 mgal contour values are observed around Amik field. Especially on Amanos Mountains contour values reach up to 80 mgal as going to West. The gravity anomaly map of the region seems simple which does not suit the tectonic informations. In Figure 9, DSF is not observed clearly, since there is alluvial covering the fault. But the effect of the western side of DSF seems to be more clearly observed. Thus we decide to apply boundary analysis and various types of the wavelet transform approach to the Bouguer gravity anomaly map. As it is known the maximum points in horizontal gradient output give the information about geological border structure. We have applied horizontal gradient in Figure 10a. We have placed pointer symbols at the maximum gradient of the coordinates using Blakely and Simpson, (1986) approach (Figure 10b). The distribution of these symbols corresponds to the geological structure of the real data.

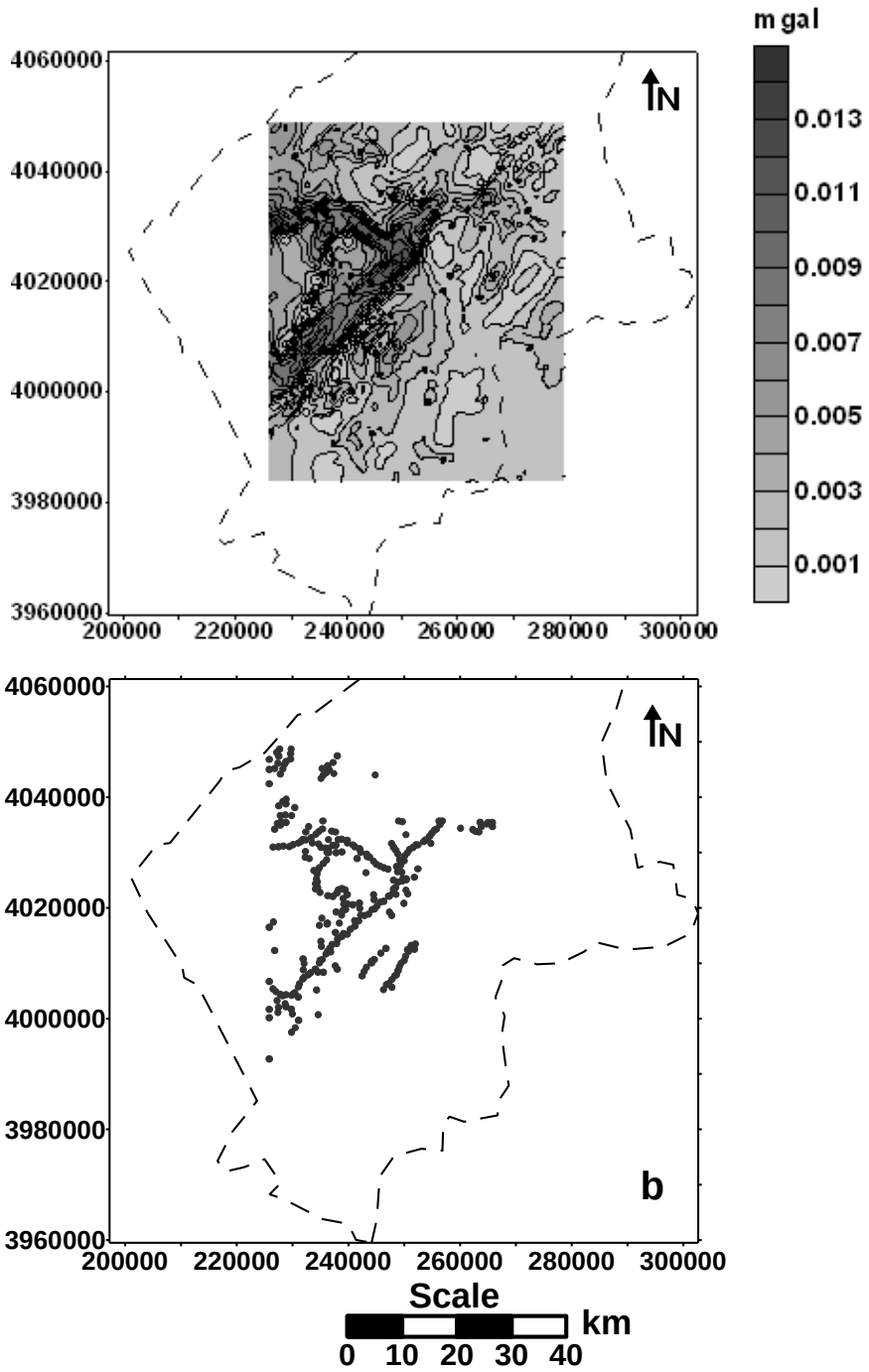

Figure 10: Horizontal gradient and boundary analysis of the Hatay Bouguer gravity anomaly map ***a.*** *Horizontal gardient* ***b.*** *Location of maximum horizontal gradient.*

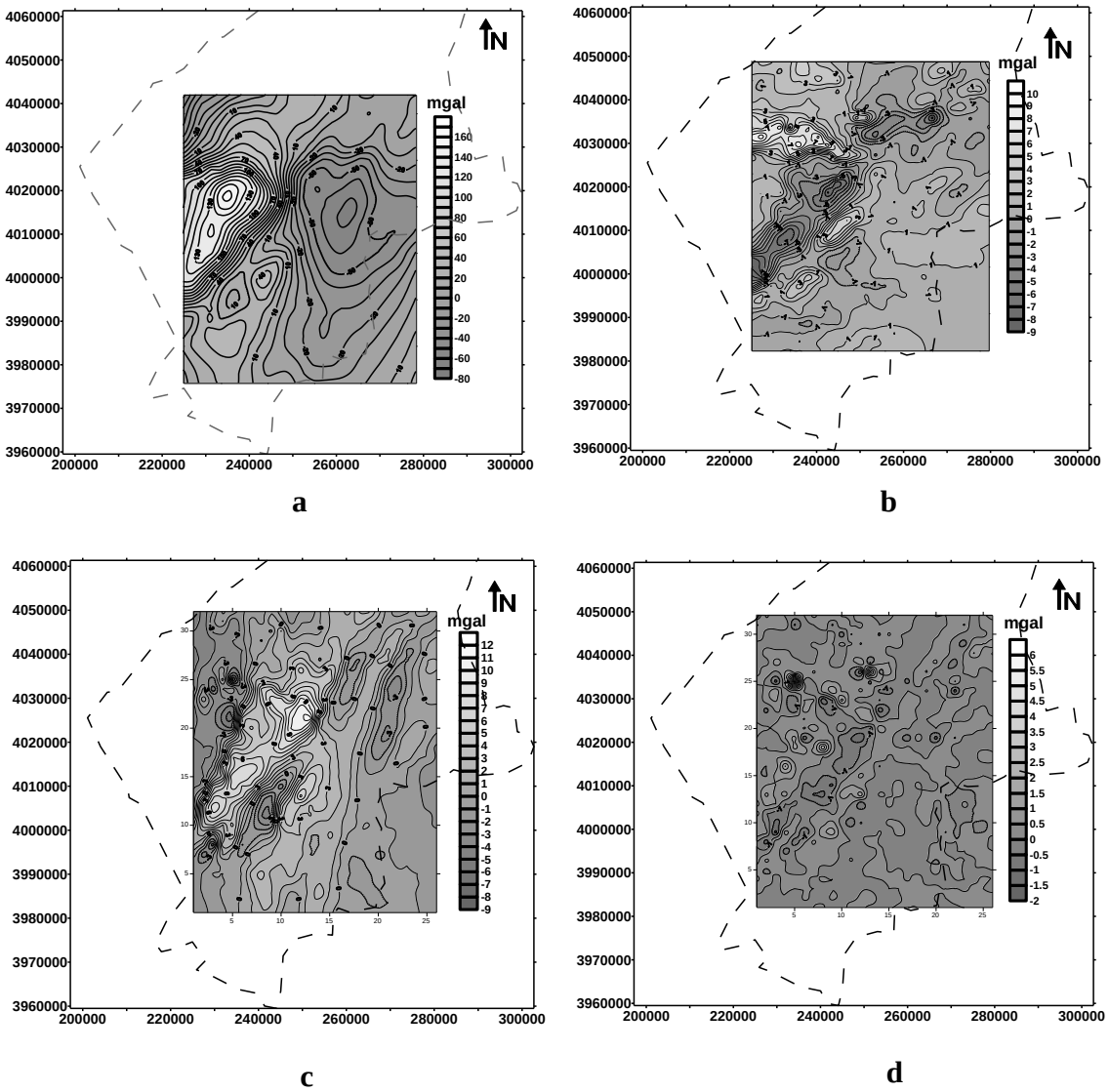

*Figure 11: Various wavelet outputs of gravity anomaly of Hatay. **(a).** approximation coefficients **(b).** horizontal **(c).** vertical **(d).** diagonal*

We have also used various types of the wavelet transform for the considered region. First order Dubaces coefficients are chosen which give the best output. The wavelet transform outputs are shown in Figure 10. Wavelet outputs of Bouguer anomaly map are given in Figure 11a. Horizontal, Vertical and Diagonal the wavelet transform outputs are as found in Figures 11b, c and d respectively. For these reason, the best result of the wavelet transform is obtained in the diagonal type of the wavelet transform (Figure 9d). Thus we can easily detect the seaside and Syria-Turkey borders.

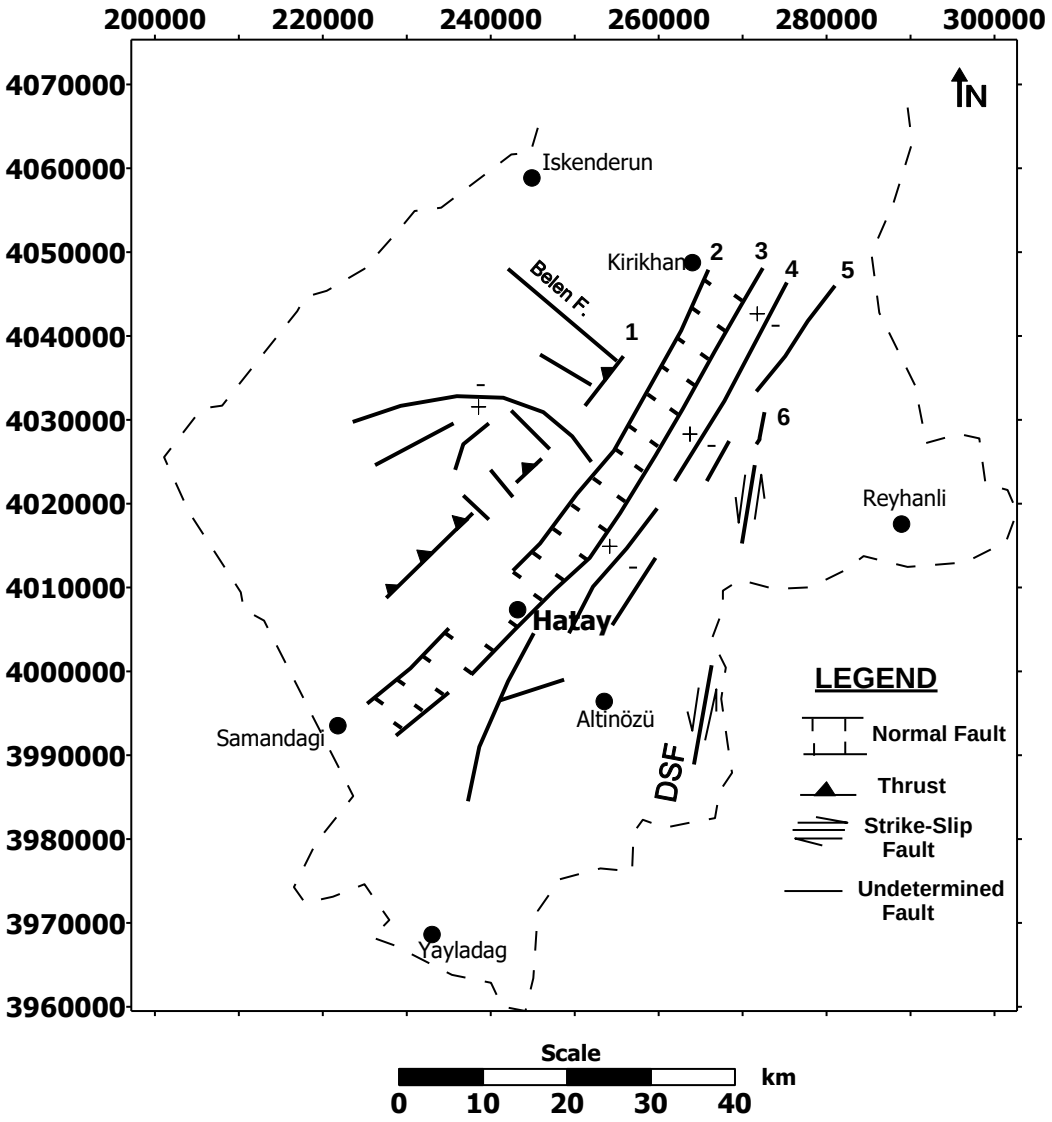

Figure 12: The proposed tectonic map of Hatay

Conclusion

There is great similarity among horizontal gradient (Figure 10) and the wavelet transform outputs (Figure 11) using geological map in Figure 6 and focal mechanisms of shallow earthquakes occurred along the Hatay region (Figure 7). The effects of structures are detected using these approaches while there are small anomalies in these coordinates of Bouguer anomaly (Figure 9). In the observation of over all tectonic structure of a complex real data as Hatay region, surface geology, classical image processing approaches on anomalies are not sufficient to solve the separation problem and modelling, thus the wavelet transform type modern techniques should be used. As an example, considering only gravity anomaly, surface geology and topography information of DSF in Hatay Region is not enough at all, since alluvioan on the surface is decreasing the effect and there seems weak anomaly at all. The modern and update vertical component of the transform application can easily estimate the effect of fault. The horizontal gradient and other the wavelet transform components, diagonal and horizontal cannot evaluate DSF fault effect. Only vertical component of wavelet results the best extraction of the property. So we can conclude that the wavelet transform, with many possible components can solve the

separation problem of real complex data better than classical derivative based approaches. Our results are compared with underground structure model of Turkish Petroleum Cooperation (TPAO) studies and they fit each other. We prepared the tectonic map of the region using all possible information obtained (Figure 12).
In the map, two main tectonic components are being separated. One of them is the DSF on the East of Hatay Region, the other fault is the graben, which lies through the Samandag-Hatay and Kirikhan direction (grabens numbered as 2 and 3 in Figure 12). We are also able to separate two normal faults parallel to graben (faults numbered as 4 and 5 in Figure 12). Since there is surface aluvians, it is not possible to separate by surface geology. An old tectonic inverse fault is also detected (fault numbered as 1 in Figure 12). Belen fault (number 6 in Figure 12) is also clearly predicted. As a result, we proposed a new model in Hatay Region, which is confirmed by different sources and geological data using an update stochastic, the wavelet transform approach.

Contributions
I thank Turkish Petroleum Cooperation (TPAO) and for their gravity data. I am also grateful to Technical Ore Research of Turkey (MTA) for their geological map.

References

[1]. Grossman A. and Morlet J. 1985. Mathematics and Physics 2, (Ed. L. Streit) World Scientific Publishing, Singapore.
[2]. Mallat, S. 1989. A Theory for Multi-resolution Signal Decomposition the Wavelet Representation, IEEE Trans. Pattern Anal. and Machine Intelligence. 31: 679-693.
[3]. Daubechies, I. 1990. The Wavelet Transform, Time-Frequency Localization and Signal Analysis, IEEE Trans, On Information Theory, 36.
[4]. Davis, A., Murshak, A., Wiscombe, W. 1994. Wavelet-base multi-fractal analysis of non-stationary and/or intermittent geophysical signals. In: Wavelets in Geophysical (eds) E. Foufoula Georgiou and P. Kumar, 249-298. Academic Press, Inc.
[5]. Chakraborty, A., Okaya, D. 1995. Frequency-time decomposition of seismic data using the wavelet transform-based methods. Geophysics. 60: 1906-1916.
[6]. Fedi M. and Quata, T., 1998. Wavelet Analysis for the regional-residual and local seperstion at potential field anomalies. Geophys. Prospect. 46: 507-525.
[7]. Hornby, P., Boschetti, F., Horovitz, F.G. 1999. Analysis of potential field data in the wavelet domain, Geophys. J. Internat. 137, 175-196.
[8]. Ridsdill-Smith, T. A., Dentith, M. C. 1999. The wavelet transform in aeromagnetic processing, Geophysics. 64: 1003-1013.
[9]. Holden, D. J., Archibald, N. J., Boschetti, F., Jessell, M.W. 2000. Inferring Geological Structures using Wavelet-Based multiscale edge analysis and forward models. Explorationa Geophysics. 31: 67-71.
[10]. Boschetti, F., Hornby, P., Horowitz, F. G. 2001. Wavelet based inversion of gravity data. Exploration Geophysics. 32: 48-55.
[11]. Ucan, O. N., Albora A. M., Hisarlı, Z. M. 2001. Comments on the Gravity and Magnetic Anomalies of Saros Bay using Wavelet approach. Mar. Geophys. Res. 22: 251-264.
[12]. Fedi, M., Florio, G. 2003. Decorrugation and removal of directional trends of magnetic fields by the wavelet transform: application to archaeological areas. Geophys. Prospect. 51: 261-272.
[13]. Albora, A. M., Hisarlı, Z. M., Ucan, O. N. 2004. Application of Wavelet Transform to Magnetic Data Due to Ruins of Hittite Civilization in Turkey. Pure Applied Geophys. 161: 907-930.
[14]. Bozkurt, E., 2001, Neotectonics of Turkey a synthesis, Geodinamica Acta 14, 3-33.
[15]. Hempton, M. R. 1987. Constraints on Arabian plate motions; an extensional history of the Red sea. Tectonics. 6: 668-705.

[16]. Arpat, E. and Saroglu, F., 1975, Some recent tectonic events in Turkey (in Turkish), Bull. Geol. Soc. Turk. 18: 91-101.
[17]. Westaway, R. and Arger, J., 1996, The Golbasi basin southern Turkey: a complex discontinuity in a major strike-slip fault zone, *J. Geol. Soc. (London)*, 153: 729-744.
[18]. Gulen, L., Barka, A. and Toksoz, M.N., 1987, Continental collision and relating complex deformation: Maras triple junction and surrounding structures, in Turkish.
[19]. Westaway, R. 2004. Kinematics of the Middle East and Eastern Mediterranean Updated. Turkish J. Earth Sci. 12: 5-46.
[20]. Williams, G. D., Unlugenc, U. C., Kelling, G., Demirkol, C. 1995. Tectonic controls on strtigraphic evolution of the Adana Basin-Turkey. Journal of the Geological Society, London. 152: 873-882.
[21]. Yurur, M. T., Chorowicz, J. 1998. Recent volcanism, tectonics and plate kinematics near the junction of the African, Arabian and Anatolian plates in the eastern Mediterranean J. Volcanol. Geoth. Res. 85: 1-15.
[22]. Rojay, B., Heimann, A., Toprak, V. 2001. Neotectonic and volcanic characteristics of the Karasu fault zone (Anatolia, Turkey): The transition zone between the Dead Sea transform and the East Anatolian fault zone. Geodın. Acta. 14: 197-212.
[23]. Over, S., Unlugenc, U. C., Ozden, S. 2001. The stres states acting in the Hatay region. Bulletin Earth Sciences Application and Research Centre of Hacettepe University. 23: 1-14.
[24]. Yurtmen, S., Guillou, H., Westaway, R. 2002. Rate of strike-slip motion on the Amanos Fault (Karasu Valley, southern Turkey) constrained by K–Ar dating and geochemical analysis of Quaternary basalts. Tectonophysics. 344: 207– 246.
[25]. Mc Kenzie, D. P. 1972. Active tectonics of the Mediterranean Region. Geophs. J. R. Astron. Soc. 30: 109-185.
[26]. Jackson, J. A., McKenzie, D. P. 1988a. The relationship between plate motions and seismic moment tensors, and the rates of active deformation in the Mediterranean and Middle East. Geophys. J. 93: 45-73.
[27]. Saroglu, F., Emre, O., Kuscu, I. 1992. The East Anatolian fault zone of Turkey. Ann. Tectonicae. VI: 99-125
[28]. Westaway, R. 1994. Present-day kinematic of the Middle East and eastern Mediterranean. J. Geophys. Res. 99: 12071-12090
[29]. Over, S., Ozden, S., Unlugenc, U. C., Yilmaz, H. 2004. A synthesis: Late Cenozoic stres field distribution at northeastern corner of the Eastern Mediterranean, SE Turkey. Geodynamics, 336: 93-103.
[30]. Blakely, R. J., Simpson, R. W. 1986. Approximating edges of source bodies from aeromagnetic or gravity anomalies. Geophysics. 51: 1494-1498.
[31]. Tekeli, O., Erendil, M. 1986. Geology and petrology of the Kizildag ophiolite (Hatay). Bulletin of the Mineral Research and Eploration. 107: 21-38
[32]. Nur, A., Ben-Avraham, Z. 1978. The eastern Mediterranean and theLevant: Tectonics of continental collision. Tectonics. 46: 297-311.
[33]. Lovelock, P. E. R. 1984. A review of the tectonics of the northern Middle-East region. Geological Magazine. 121: 577-587.
[34]. Ambraseys, N. N., Barazangi, M. 1989. The 1795 earthquake in the Bekaa Valley: Implications for earthquake hazard assessment in the eastern Mediterranean region. J. Geophys. Res. 94: 4007-4013.
[35]. Kenzie, D. P. 1978. Active tectonics of the Alpine-Himallyan belt: the Aegean Sea and surrounding regions (tectonics of Aegean region). Geophs. J. R. Astron. Soc. 55: 217-254.
[36]. Jackson, J., McKenzie, D. P. 1988b. Active tectonics of the Alpine-Himalayan belt between western Turkey and Pakistan. Geophs. J. R. Astron. Soc. 77: 185-264.

[37]. Lybéris, N., Yurur, T., Chorowicz, J., Kasapoglu, K.E., Gundogdu, N. 1992. The East Anatolian Fault: an oblique collisional belt. Tectonophysics. 204: 1-15.
[38]. Klinger, Y., Avouac, J. P., Abou, K. N., Dorbath, L., Bourles, D., Reyss, J. L. 2000. Slip rate on the Dead Sea transform fault in northern Arava Valley (Jordan). Geophys. J. Int. 142: 755-768.
[39]. Perincek, D., Cemen, I. 1990. The structural relationship between the East Anatolian Fault and Dead Sea Fault zones in southern Turkey. Tectonophsics. 172: 331-340.
[40]. Albora, A. M. 1998. Investigation of gravity density distribution in Hatay area. Ph. D. thesis, Istanbul Univ., Science Inst., Istanbul.
[41]. Demirel, S. 1993. Evaluation of the geophysical data on Iskenderun Bay (in Turkish), Istanbul University, Science Institute, Ph D thesis.
[42]. Gunay, Y. 1994. Geology of Amanos Mountains and petrol potentiality of Karasu -Hatay Graben System. General Directorate of Research Grup, Raport No:1954 .
[43]. General Directorate of Mineral Research and Exploration
[44]. Eyidogan, H. 1983. Seismotectonic Properties of Bitlis -Zagros Thrust belt (İn Turkish), PhD thesis, Istanbul Tech. Univ. Fac. Minning, Istanbul.
[45]. Taymaz, T., Eyidoğan, H., Jackson, J. 1991. Source parameters of large earthquakes in the East Anatolian Fault Zone (Turkey). Geophys. J. Int. 106: 537-550.
[46]. Tan O. 2023. Earthquake Watch: The 6 February 2023 Kahramanmaraş Earthquakes – A catastrophic day for Turkey. EGU 03.04.2023.
[47]. https://www.mta.gov.tr/files/img/popup/2023